Applied Chemical Engineering (2025) Volume 8 Issue 1 ISSN: 2578-2010 (O)
doi: 10.59429/ace.v8i1.5604

RESEARCH ARTICLE

Synthesis, characterization and adsorption properties of azo-functionalized polymeric hydrogels for R6G dye removal from water

Amna N. Zghair[1], Ziyad T. Al-Khateeb[2], Layth S. Jasim[3*], Maryam Batool[4]

[1] *Ministry of Education General Directorate of Al-Qadisiyah Education, Diwaniyah, 58001, Iraq*
[2] *Department of Chemistry, College of Science, University of Al-Qadisiyah, 58001, Diwaniya, 58001, Iraq*
[3] *Department of Chemistry, College of Education, University of Al-Qadisiyah, Diwaniyah, 58001, Iraq*
[4] *Department of Chemistry, University of Sahiwal, Sahiwal, 57000, Pakistan*
***Corresponding author:** Layth S. Jasim, layth.alhayder@qu.edu.iq

ABSTRACT

In this study, 2- [2-(5-Chloro carboxy phenyl) azo] 1-methyl imidazole (1-MeCPAI) was synthesized and used in developing hydrogels via free radical polymerization with acrylic acid (AA) and N, N-methylene bisacrylamide. The synthesized P(AA-co-1-MeCPAI) hydrogels were evaluated for their effectiveness in adsorbing R6G dye from aqueous solutions. The characterization of these hydrogels included techniques as Fourier Transform Infrared Spectroscopy (FTIR), Thermal Gravimetric Analysis (TGA), BET (Brunauer-Emmett-Teller) and BJH (Barrett-Joyner-Halenda) analysis, X-ray diffraction (XRD), and Field Emission Scanning Electron Microscopy (FESEM). The study revealed that adsorption efficiency is influenced by pH, temperature, contact time, and adsorbent dose, with adsorption following a pseudo-second-order kinetic model and best fitting the Temkin isotherm, indicating a multilayer adsorption process. Thermodynamic analysis confirmed that the process is exothermic and spontaneous, underscoring the potential of P(AA-co-1-MeCPAI) hydrogels as effective adsorbents for dye removal.

Keywords: Hydrogels; R6G dye; characterization; batch adsorption; water treatment

ARTICLE INFO

Received: 9 January 2025
Accepted: 10 February 2025
Available online: 14 February 2025

COPYRIGHT

Copyright © 2025 by author(s).
Applied Chemical Engineering is published by Arts and Science Press Pte. Ltd. This work is licensed under the Creative Commons Attribution-NonCommercial 4.0 International License (CC BY 4.0).
https://creativecommons.org/licenses/by/4.0/

1. Introduction

The presence of various contaminants in water, such as paints, dyes, and pesticides, metals, pharmaceutical products, microorganisms [1-3], and others, presents a complex challenge [1,4-5]. These pollutants contribute to numerous diseases that pose significant risks to human health. Many dyes are resistant to degradation [6-8]. Industrial dyes, widely used in products such as paper, plastics, textiles, food, and cosmetics, are considered major water contaminants. Globally, over seven million tons of these pigments are produced annually. These pigments consist of a variety of chemicals, the environmental impact of which is largely unknown. Approximately 10-15% of these dyes are lost as industrial wastewater, which is often discharged into water bodies or soil, posing significant health risks to plants, animals, and humans[9]. These dyes are bioaccumulative and resistant to degradation by oxygen and sunlight. Consequently, dyes in wastewater are considered undesirable, necessitating their removal from water sources prior to environmental release. This is crucial not only for ecological reasons but also due to their toxicity and long-term effects on both the environment and

human health [10].

Several physical and chemical methods, including ultrasonic irradiation, ion exchange, biological treatment, membrane separation, and sorption explored to mitigate pollution and its associated challenges [11]. Research has shown that certain materials exhibit a high absorption capacity for organic substances, including water contaminants and dyes. While numerous systems utilizing adsorption techniques have been developed in recent years, achieving cost-effective dye removal continues to be a significant challenge[12-16]. In the present study, efforts were made to synthesize novel azo-functional polymeric hydrogels derived from 2-[2-(5-Chloro carboxy phenyl) azo] 1-methyl imidazole (1-MeCPAI) and acrylic acid (AA) through free radical polymerization for the purpose of R6G dye removal. Additionally, techniques including AFM, FESEM, FTIR, BET/ BJH analysis, and TGA were employed to study dye adsorption on synthesized hydrogels. The novelty of this work lies in the synthesis of a previously unexplored hydrogel that has not been used previously for R6G dye adsorption from water.

2. Materials and methods

2.1. Chemicals and materials

Acrylic acid was obtained from Himedia (India). Potassium persulfate (KPS), was supplied by Merck (Germany), while the multifunctional crosslinker, N, N'-methylene bisacrylamide (NMBA) supplied via Fluka, Germany. All other chemicals used were of analytical grade and were utilized without further purification. The compound 2-[2-(5-Chloro carboxy phenyl) azo] 1-methyl imidazole (1-MeCPAI) was synthesized as described in the literature [17]. Percentage purity of R6G dye used was 99.5%. All solutions were prepared using deionized water.

2.2. Preparation of P (1-MeCPAI-co-AA) hydrogels

Poly (AA-co-1-MeCPAI) hydrogels were synthesized through free radical copolymerization. The monomers (AA and 1-MeCPAI) were dissolved in 4 mL distilled water. To this solution, 1 mL of a 2 wt% MBA crosslinking agent and 1 mL of a 5 wt% potassium persulfate solution were added. The free radical polymerization was conducted in a 50 mL beaker, maintained at 60°C, to ensure complete matrix formation [18]. The schematic representation of the chemical reaction for the formation of P(AA-co-1-MeCPAI) hydrogels is provided in **Figure 1.**

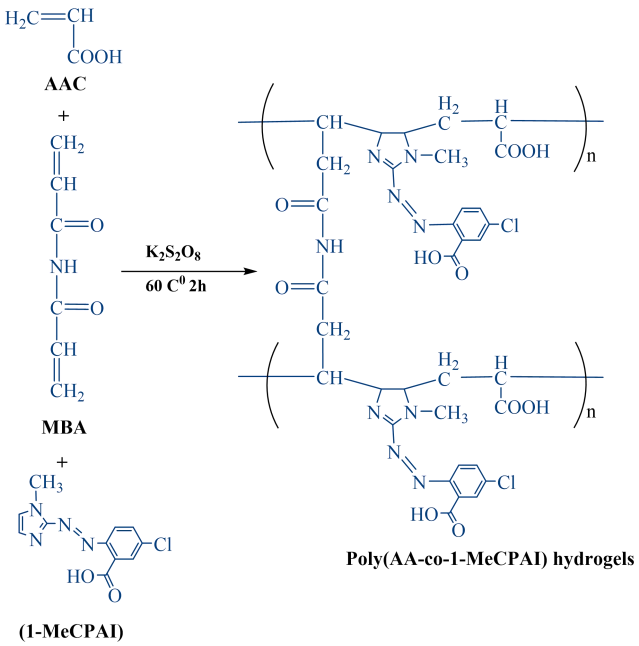

Figure 1. Synthesis of P(AA-co-1-MeCPAI) hydrogels.

3. Results and discussion

3.1. Characterization results

3.1.1. FTIR results

The FTIR spectrum of prepared hydrogel is shown in **Figure 2(a).** The compound exhibits an orange color, 87 % yield and a melting point of 192 °C. FTIR analysis (using KBr disc) reveals absorption peaks at 3277 cm^{-1} corresponding to the O-H stretch, 3101 cm^{-1} for the HC=CH stretch, and 1717 cm^{-1} associated with the C=O stretch. The infrared spectra of P(AA-co-1-MeCPAI) before and after adsorption, shown in **Figure 2(b)** and **2(c),** display a broad absorption band within the range of 3187–3510 cm^{-1}. This broadening indicates overlap between OH stretch and -NH stretch. Bands observed at 2800–2943 cm^{-1} correspond to the stretching vibrations of CH_2-CH_3 groups, indicating the presence of -CH bonds. Additionally, the bands within the range of 1676–1740 cm^{-1} confirmed carbonyl (C=O) groups. The bands between 1020–1430 cm^{-1} are attributed to vibrations of C-N, C-O, and C-C bonds (19).

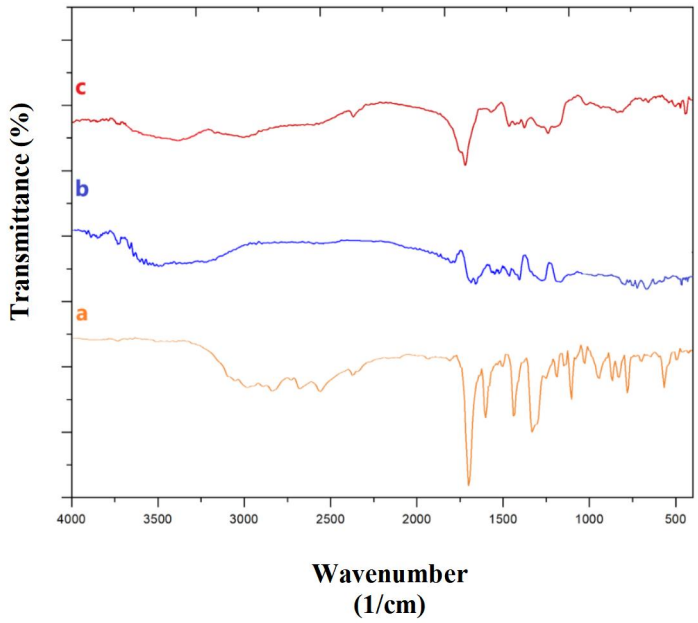

Figure 2. FTIR spectra of (a) 1-MeCPAI organic reagent, P(AA-co-1-MeCPAI) hydrogels (b) before and (c) after dye adsorption.

3.1.2. XRD results

The X-ray diffraction (XRD) patterns of P(AA-co-1-MeCPAI) hydrogel and the 1-MeCPAI organic reagent are shown in **Figure 3.** These results indicate the crystalline nature of the organic reagent prior to its incorporation into the hydrogel. The 1-MeCPAI exhibits three characteristic intense peaks at 2θ values of 18°, 24°, and 27°, which are indicative of its crystalline structure. However, after incorporation into the hydrogel, these peaks are no longer observed, suggesting that 1-MeCPAI is molecularly dispersed within the hydrogel network, and no crystalline structures remain in the 1-MeCPAI-loaded hydrogel[19-21].

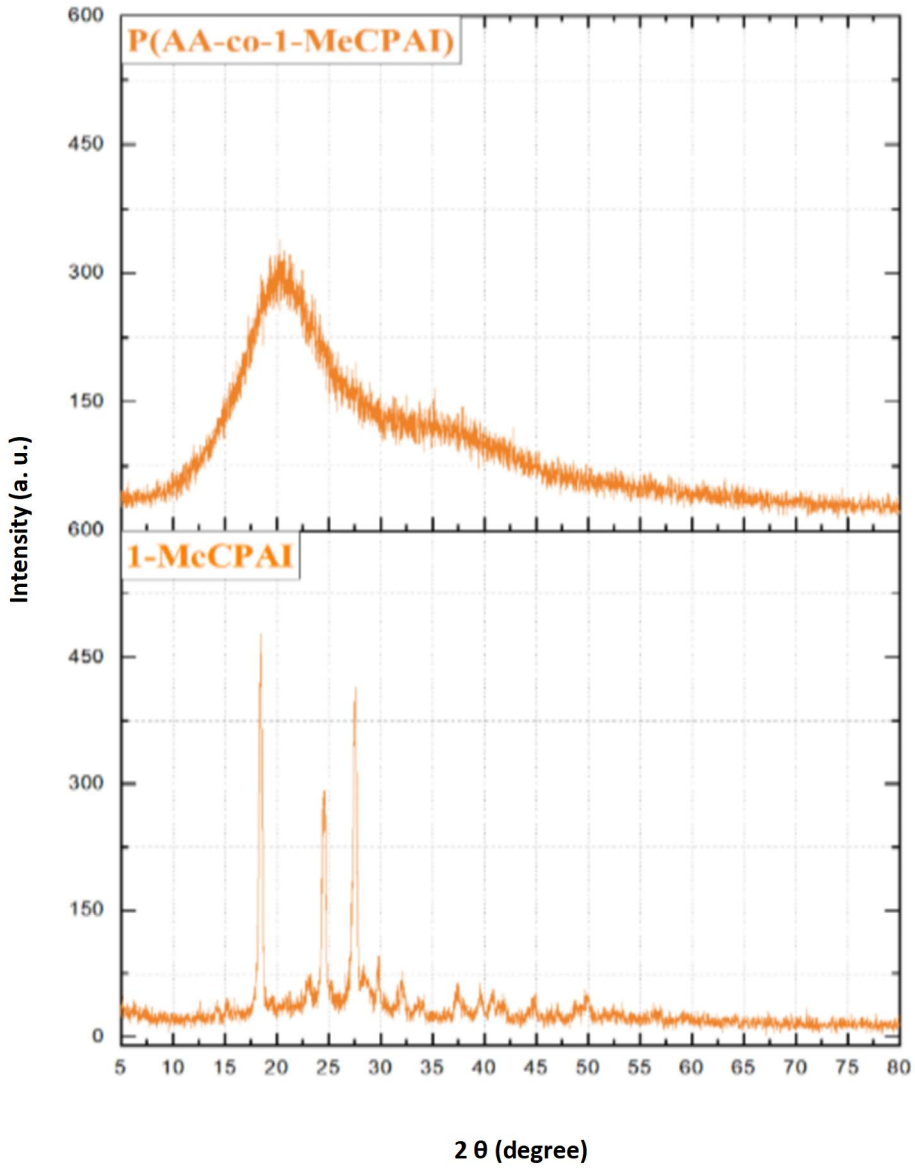

Figure 3. XRD pattern of 1-MeCPAI organic reagent and P(AA-co-1-MeCPAI) hydrogels.

3.1.3. TGA results

The thermal stability of prepared P(AA-co-1-MeCPAI) hydrogels was assessed using thermogravimetric analysis (TGA). As shown in **Figure 4,** the weight loss of the hydrogel occurred in three distinct stages. In the first stage, between 30.26 °C and 211.28 °C, a weight loss of approximately 6.964 % was observed, attributed to the loss of water molecules adsorbed on the surface. The second stage of decomposition occurred between 211.28 °C and 346.66 °C, with a remaining weight of 48.984 %, indicating a weight loss of 44.05 % due to the decomposition of carboxyl groups, releasing CO molecules. However, in third stage, from 346.66 °C to 483.77 °C, the remaining mass was 16.10 %, with a weight loss of 32.884 %. This can be attributed to the breakdown of the hydrogel's compact structural network. These results demonstrate that the P(AA-co-1-MeCPAI) hydrogels exhibit good thermal stability [22].

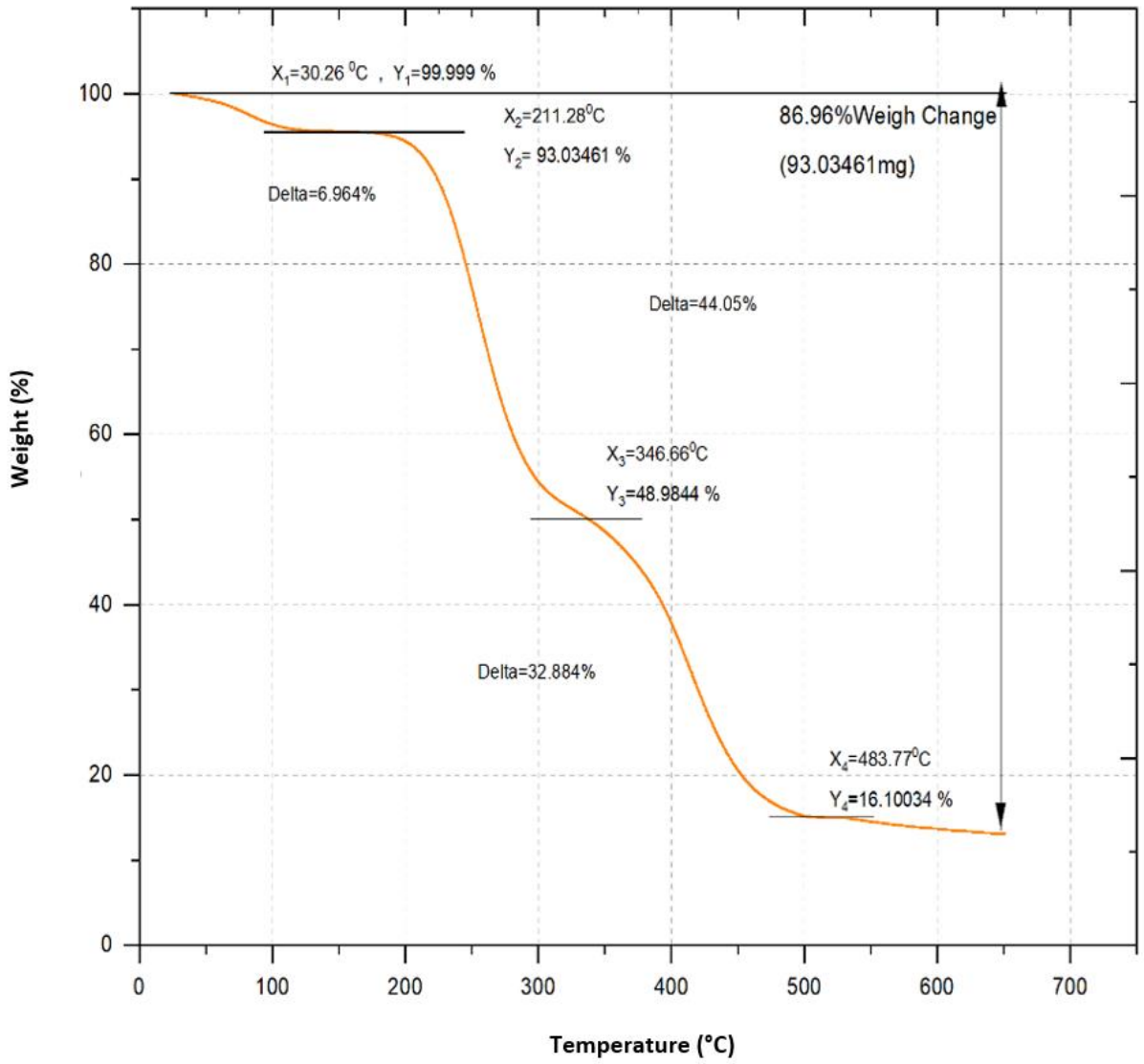

Figure 4. TGA curve of P(AA-co-1-MeCPAI) hydrogels.

3.1.4. BET results

BET analysis was conducted to estimate the surface area and pore volume of prepared hydrogels before and after adsorption, using nitrogen adsorption/ desorption isotherms measured at 77 K, as shown in **Figure 5a-d.** According to IUPAC classification, the isotherms for P(AA-co-1-MeCPAI) (**Figure 5a-b**) can be classified as type IV, with H2-type hysteresis loops, which corresponds to non-rigid aggregates or assemblages of slit-shaped pores in hydrogel. The specific surface area, total pore volume, and mean pore diameter obtained from BET analysis were 3.5665 m^2/g, 0.00043 cm^3/g, and 4.919 nm, respectively. After the adsorption of dye, the total pore volume and mean pore diameter, as determined by BJH analysis (**Figure c-d**), were 0.00091 cm^3/g and 5.065 nm, correspondingly[23].

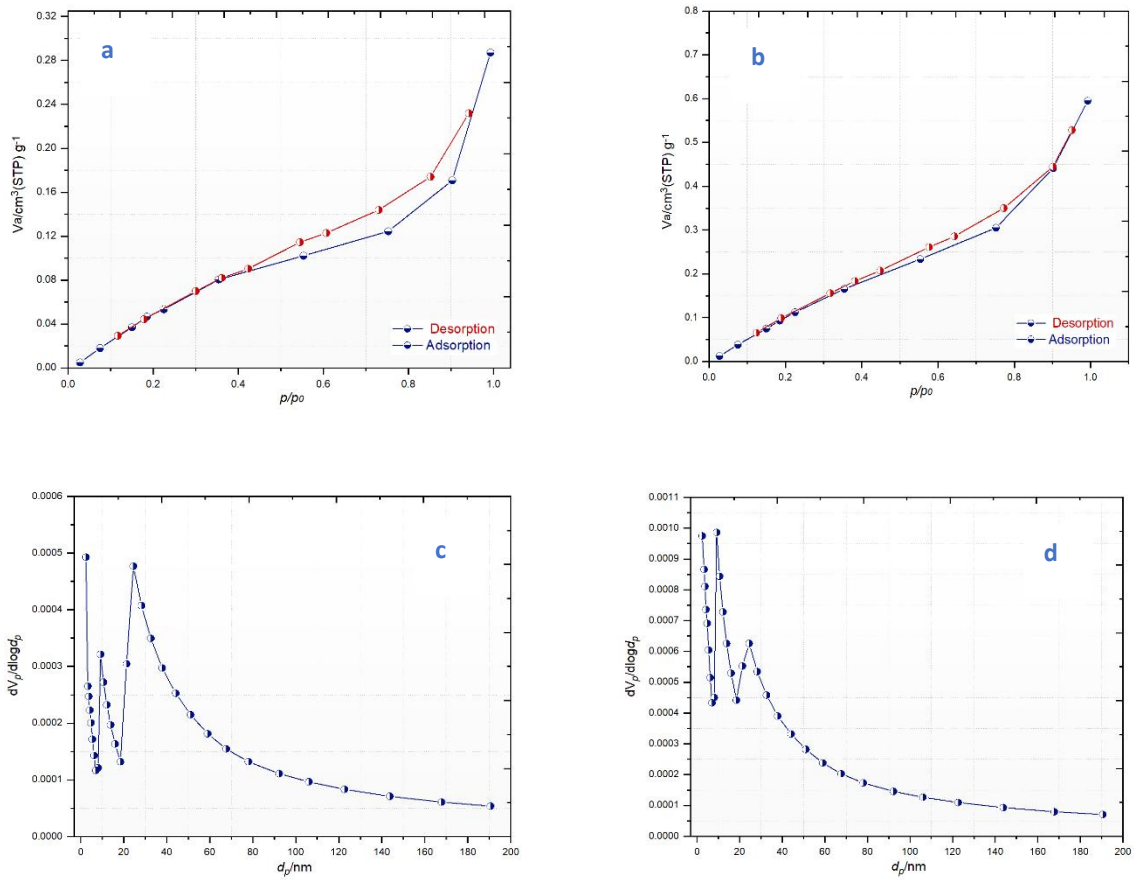

Figure 5. (a) and (b) BET isotherms, (c) and (d) BJH pore size distribution curves before and after dye adsorption respectively.

3.1.5. FESEM results

FE-SEM used to analyze morphology of P(AA-co-1-MeCPAI) hydrogels. The FE-SEM images before adsorption (**Figure 6a**) revealed that the hydrogel sheets exhibit a closely aligned layered structure, forming stacked thick layers. The hydrogels tend to aggregate, creating multilayer agglomerates. After adsorption of dye (**Figure 6b**), the surface of hydrogels becomes roughened, with the dyes appearing uniformly distributed across the surface, visible as bright dots, as shown in **Figure 6.**

3.2. Zero-point charge (pH_{zpc}) of hydrogel

The determination of point of zero charge (pH_{zpc}) is essential in understanding the adsorption behavior of hydrogel composite. This point can be identified on the graph where the axes intersect. Results illustrated in **Figure 7** reveal that the hydrogel composite reaches a neutral charge at a pH of 5. When the pH is below the pH_{zpc}, or less than 5, the surface of the adsorbent material becomes positively charged. This resulted in developing hydrogen bonding between positively charged surface groups. This interaction causes surface molecule contraction and a reduction in swelling ratio, significantly limiting the diffusion of cationic pollutants into the surface. Consequently, electrostatic repulsion between the positively charged hydrogel composite surface and cationic pollutants decreases the adsorption efficiency. Optimal adsorption occurs when the pH exceeds the pH_{zpc}, meaning when it is greater than 5. In this case, surface functional groups such as carbonyl, carboxyl, and hydroxyl groups lose protons and become ionized, leading to a negatively charged surface. This ionization increases the distance between the polymer chains on the surface, enhancing the swelling ratio. Consequently, the diffusion of cationic pollutants into the surface improves, while electrostatic attraction between the negatively charged adsorbent surface and cationic pollutants further enhances adsorption efficiency[10].

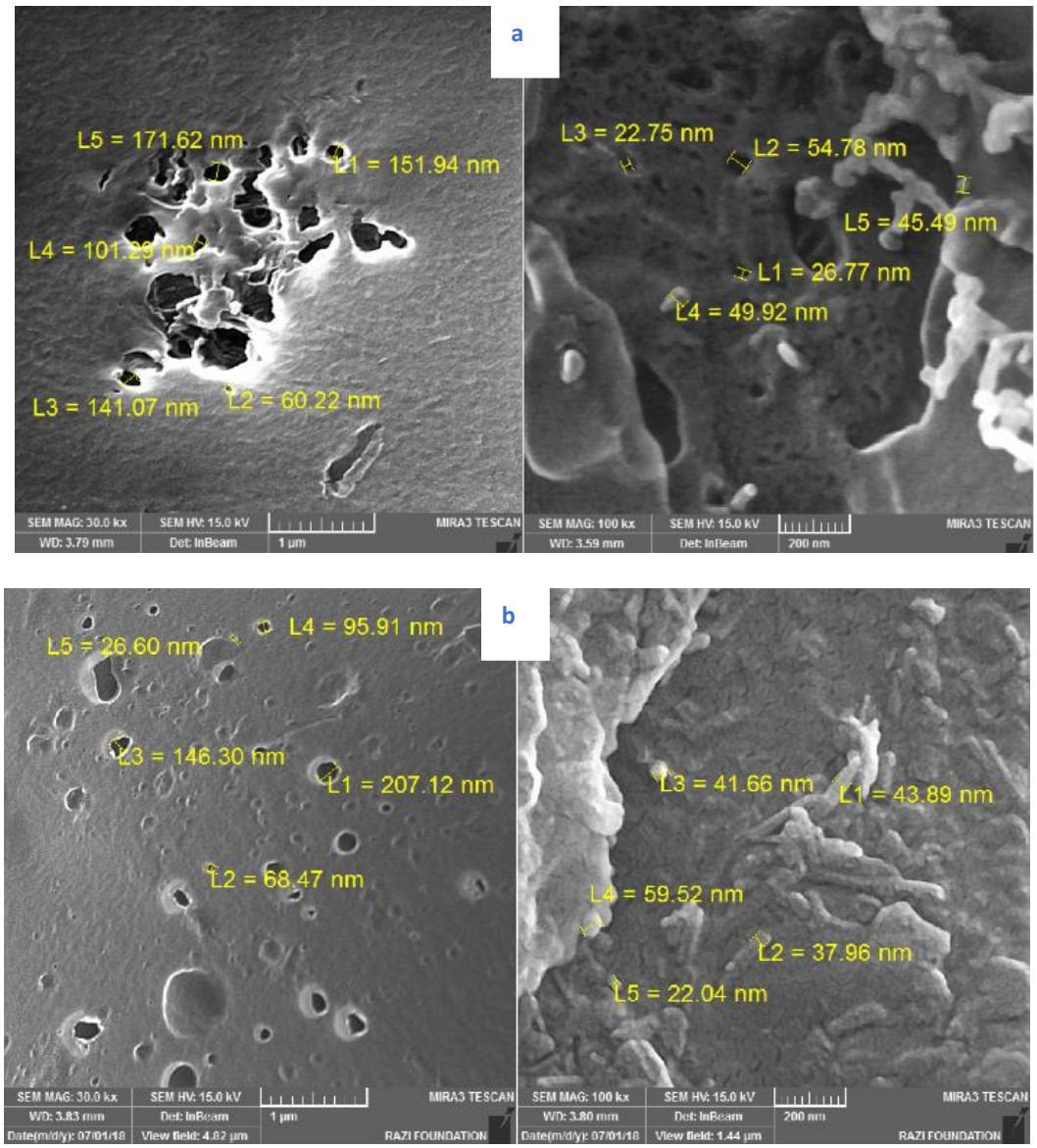

Figure 6. FE-SEM images of P(AA-co-1-MeCPAI) hydrogels (a) before and (b) after dye adsorption.

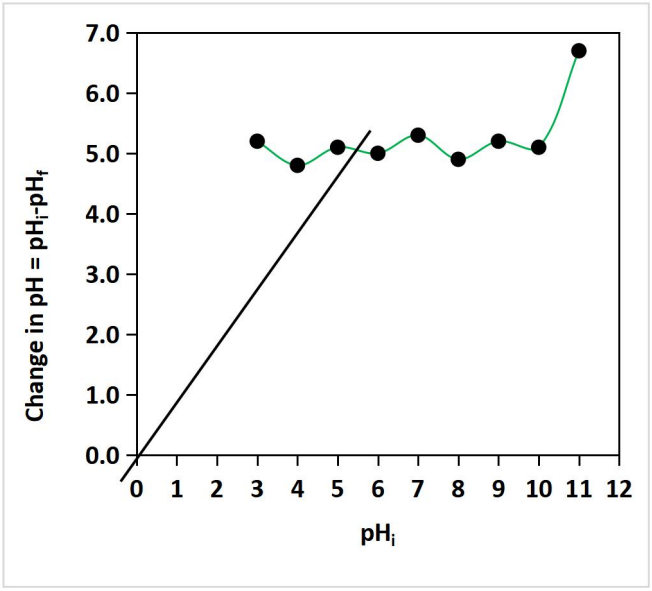

Figure 7. Point of zero charge (pHzpc) of P(AA-co-1-MeCPAI) hydrogel.

3.3. Effect of adsorbent dose and pH

Various weights of the prepared hydrogel composite (0.001 g/10 mL to 0.15 g/10 mL), employed for 1000 ppm dye concentration. A 10 mL dye solution was added to each studied weight of hydrogel, maintaining a temperature of 25 ˚C. The results, Figure 8, indicate that the adsorption capacity increases with hydrogel dose due to an increase in surface area and thereby availability of free active sites. This, in turn, enhances the adsorption capacity for dye molecules on hydrogel surface reaching maximum at adsorbent dose of 0.15 g/10 mL. Since no significant variation was observed in adsorption capacity while using 0.05 g/10 mL and 0.15 g/10 mL, therefore, an optimal adsorbent dose of 0.05 g/10 mL was identified for effective adsorption[24].

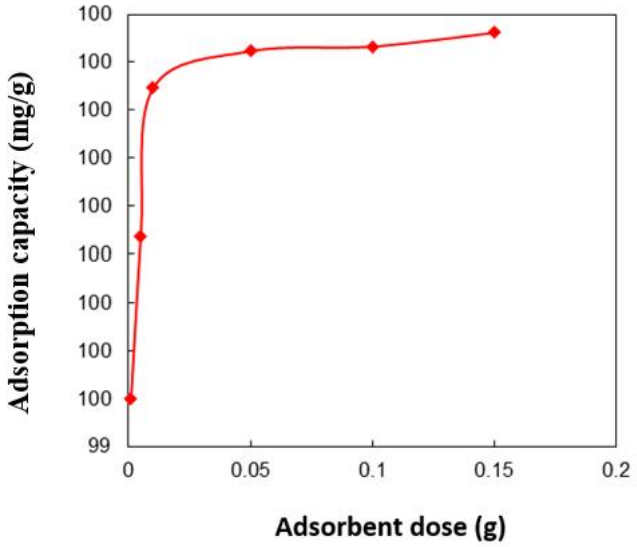

Figure 8. Effect of adsorbent dose.

The impact of pH on adsorption of R6G dye onto hydrogel surface studied at a dye concentration of 1000 ppm across pH values ranging from 2 to 10. A fixed adsorbent dose of 0.05 g per 10 mL of dye solution was used, with optimal conditions of 25 °C and 150 min. The results, shown in **Figure 9**, indicate that quantity of dye adsorbed on hydrogel increases with an increase in pH but upto a certain limit. The lowest adsorption efficiency at pH 2 and the highest capacity was observed at pH 10. The increase in adsorption with higher pH is attributed to the ionization of carboxyl and hydroxyl groups on adsorbent surface, which lose protons and become negatively charged. This raises the concentration of hydroxide ions (OH^-) in solution, making the adsorbent surface negatively charged. Consequently, hydrogel surface undergoes swelling and expansion, enhancing the electrostatic attraction between dye molecules and negatively charged composite surface. This increased attraction facilitates the diffusion of dye molecules on hydrogel surface, thereby improving adsorption efficiency. Lower pH reduces adsorption due to fewer negatively charged sites on hydrogel, repelling positively charged dye molecules. This electrostatic repulsion limits the adsorption capacity[25].

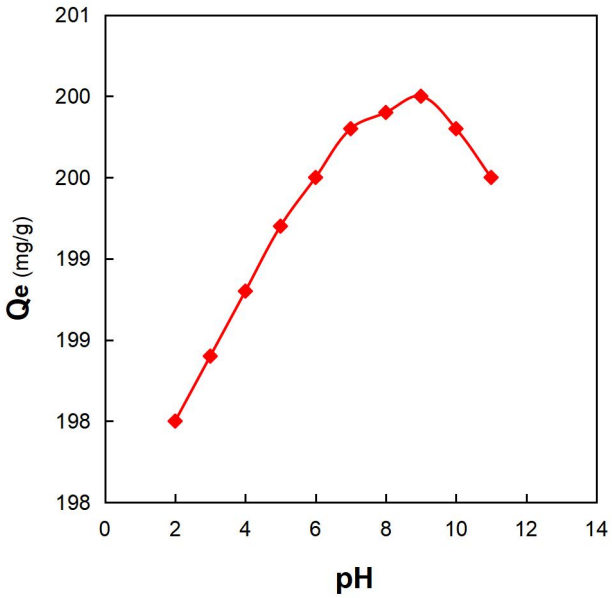

Figure 9. Effect of pH on R6G dye adsorption.

3.4. Effect of temperature

The dye adsorption on hydrogel studied at different temperatures (20, 25, 30, and 35 ˚C) and within a fixed concentration range (400-1000 ppm). Changes in temperature can either enhance or reduce the adsorbent's ability to capture dyes from aqueous solutions. The results for R6G dye adsorption, depicted in Figure 10, indicate a decrease in the amount of dye adsorbed as temperature increases, confirming that the adsorption process is exothermic. This decrease is attributed to the increased solubility of the dye particles in solvent at elevated temperatures, thereby reducing the affinity of dye particles for adsorbent surface. Additionally, higher temperatures increase the kinetic energy of adsorbed molecules on hydrogel surface, leading to an increase in system entropy (ΔS) as mobility of adsorbed molecules on hydrogel surface decreases. This reduction in attraction between dye molecules and active sites on adsorbent surface results in decreasing the adsorption force[25].

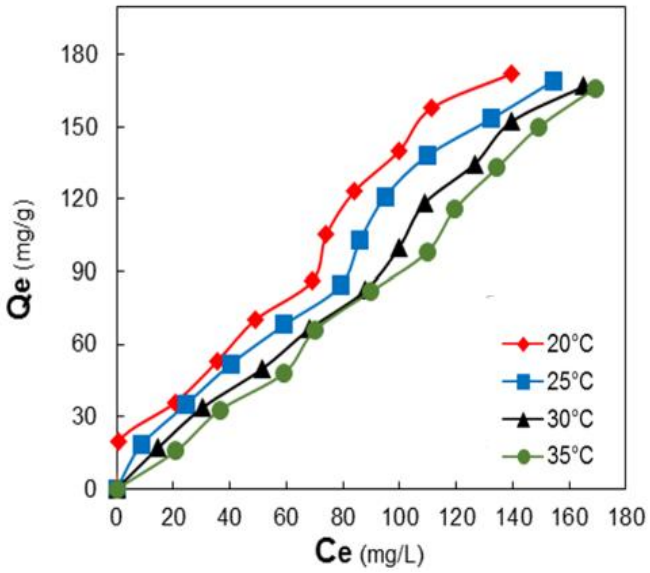

Figure 10. Effect of temperature on R6G dye adsorption.

Thermodynamic functions i.e., change in Gibb's free energy (ΔG), enthalpy (ΔH), entropy (ΔS) ($\Delta G = \Delta H - T\Delta S$) were calculated as they are essential for interpreting various reactions, especially in adsorption process. These functions allow for determining the reaction direction, nature of controlling forces (whether physical or chemical), and provide valuable insight into the organization of molecules within systems resulting from molecular interactions. The enthalpy change (ΔH) is a key measure of interaction strength between dye molecules and adsorbent surface. The value of ΔH for dye adsorption on grafted hydrogel surface was obtained by plotting (ln X_m) against the reciprocal of absolute temperature (1/T), resulting in a straight line. From the slope of this line (slope = -R/ΔH), enthalpy of dye adsorption on hydrogel composite surface was determined, as illustrated in **Figure 11.**

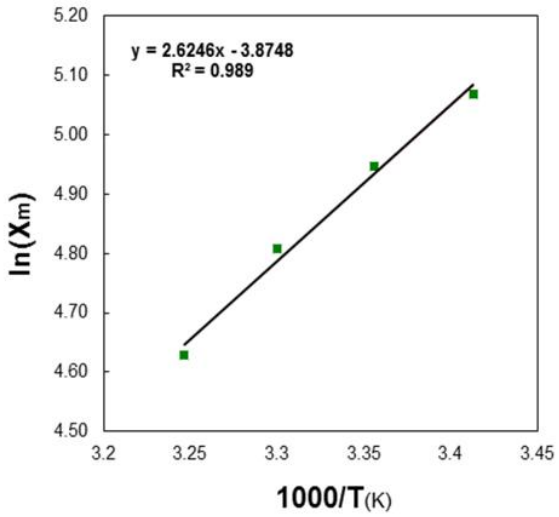

Figure 11. A plot of ln X_m against inverse absolute temperature for R6G dye adsorption.

The calculated thermodynamic parameters in **Table 1** for the dye adsorption process revealed negative enthalpy change (ΔH) that showed exothermic nature of R6G dye adsorption. This suggests that interaction between adsorbent surface and dye molecules decreases with increasing temperature, likely due to the breaking of bonds formed between active sites of adsorbent and dye molecules. Additionally, the negative Gibbs free energy change (ΔG) confirms the spontaneous nature of adsorption process. The positive entropy change (ΔS) indicates that the molecules are in constant, random motion. Given that the enthalpy change (ΔH) is less than 40 kJ/mol, the adsorption is characterized as physical adsorption[19,26].

Table 1. Thermodynamic parameters for adsorption of R6G dye on surface.

T (°C)	ΔG (kJ/mol)	ΔH (kJ/mol)	ΔS (J/mol K)
20	-13.43	-0.08	45.89
25	-13.69		45.95
30	-13.88		44.89
35	-13.91		43.88

3.5. Adsorption isotherms

Adsorption isotherms were studied to describe the interaction between dye adsorbed (Q_e (mg/g)) on hydrogel and its equilibrium concentration (C_e (mg/L)). Based on the data obtained and Giles' classification, the results indicate that adsorption of R6G dye corresponds to 'S' type, suggesting multilayer adsorption. Additionally, solvent may experience strong adsorption on the adsorbent surface. The Langmuir isotherm supposes that the adsorption takes place at specified and homogeneous adsorbent surface (chemical sorption). The Freundlich model indicates that the adsorption physical adsorption). Langmuir (Equation 1), Freundlich

(Equation 2), and Temkin (Equation 3) isotherm models were applied to describe the adsorption characteristics of adsorbents used for dye removal from the environment.

$$\frac{C_e}{q_t} = \frac{C_e}{q_{max}} + \frac{1}{q_o b} \quad (1)$$

here, constant of Langmuir model and maximal capacity is expressed by b (L/mg) and q_{max} (mg/g) correspondingly.

$$\ln q_t = \ln K_f + \frac{1}{n} \ln C_e \quad (2)$$

here, Freundlich constant as well as exponent (mg/g) referred as K_f and 'n' correspondingly.

$$q_{eq} = B \ln A_T + B \ln C_{eq} \quad (3)$$

here, R and B denotes constant of universal gas (J/mol K) and adsorption heat (J/mol), A_T and T denotes constant of Temkin equilibrium binding (L/ g) and absolute temperature (K) correspondingly. As presented in **Table 2** and **Figure 12**, the Temkin isotherm aligns closely with the adsorption of R6G dye, as evidenced by the correlation coefficient R^2, which is 0.9865. The conformity with the Freundlich isotherm (R^2 = 0.9764) indicates multilayer adsorption, reflecting the heterogeneous nature of surface and varied energy of active sites on hydrogel surface. Conversely, the Temkin isotherm suggests that adsorption occurs as a thick monolayer of adsorbed molecules[27].

3.6. Kinetic study

The time required for equilibrium of R6G dye on hydrogel was investigated at a constant concentration of 1000 ppm, temperature of 25 °C, and pH of 7, over various time intervals ranging from 1 min to 180 min, using a fixed hydrogel weight of 0.05 g. The results, illustrated in **Figure 13**, showed that equilibrium for R6G dye adsorption was achieved at 150 minutes on the grafted hydrogel surface. Study revealed that adsorption of dye on prepared hydrogel surface first increases with time, exhibiting a very rapid rate within the first 20 minutes. This initial rapid adsorption is due to availability of numerous active sites on the composite surface. As time progresses, the amount of adsorbed dye reaches equilibrium, where adsorption begins to slow down, attributed to the occupation of the majority of active sites by dye molecules. Consequently, adsorption becomes more challenging as most active sites on the adsorbent surface were occupied by R6G dye molecules[27].

Table 2. Parameters of Langmuir, Freundlich and Temkin models for R6G dye adsorption.

Langmuir	**Freundlich**	**Temkin**
q_0 (mg/ g)	**K_f (mg g^{-1})**	**B (J/mol)**
277.77	95.94	66.45
b (L/g)	**n**	**A_T (L/g)**
0.51	1.98	4.23
	R^2	
0.98	0.97	0.98

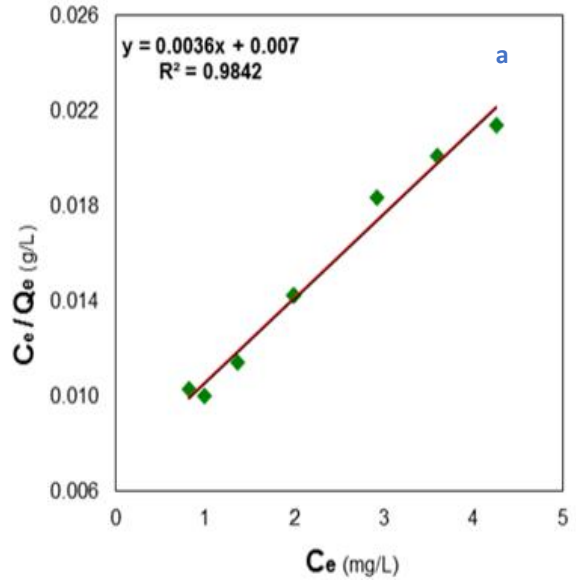

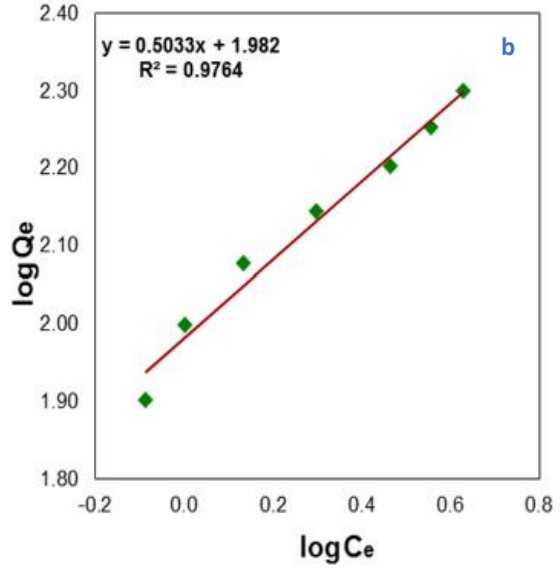

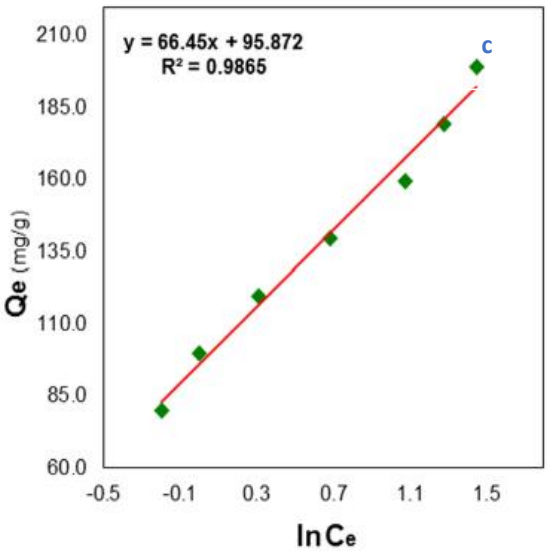

Figure 12. (a) Langmuir, (b) Freundlich and (c) Temkin models.

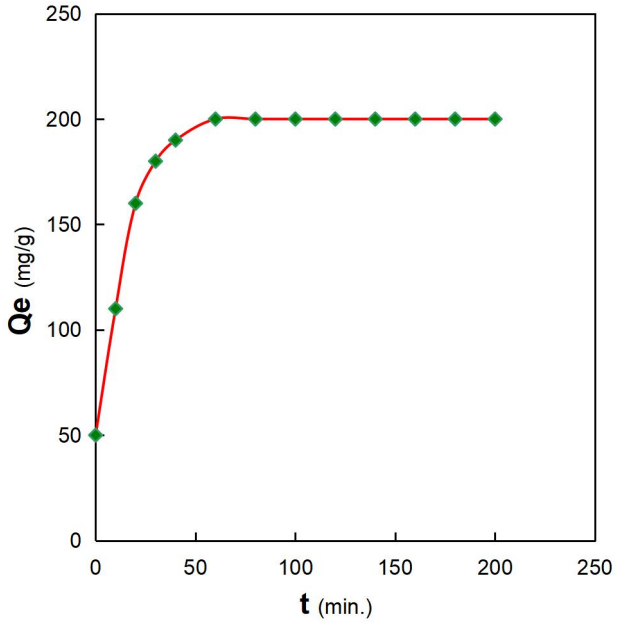

Figure 13. Effect of time on amount of R6G dye adsorbed.

Studying adsorption kinetics is essential for determining the time required for the adsorption process to reach equilibrium, beyond which adsorption stops/ constant. The kinetic models for R6G dye adsorption on hydrogel surface were examined at a fixed concentration of 1000 ppm and a temperature of 25 °C, where adsorption rate fluctuates over time. Kinetic models were employed to analyze the experimental data, with the most commonly applied models being the pseudo-first-order (Equation 4) and pseudo-second-order (Equation 5) models, as illustrated in **Figure 14.**

$$\log(Q_e - Q_t) = \log Q_e - \frac{k_1}{2.303}t \quad (4)$$

$$\frac{t}{Q_t} = \frac{1}{k_2 Q_e^2} + \frac{t}{Q_e} \quad (5)$$

here Q_t (mg/g), Q_e (mg/g) is amount of adsorbed dye after time t (min) and at equilibrium, correspondingly. k_1 (1/min) and k_2 (g/mg·min) refers to rate constant for pseudo-first as well as second model correspondingly[28]. Using these models, kinetic constants and correlation coefficients (R^2) were calculated for each model. The results (**Table 3**) indicated that the R^2 value for the pseudo-second-order model was higher than that for the pseudo-first-order model for R6G dye adsorption. Thus, it was concluded that the adsorption process follows the pseudo-second-order model highlighting chemical adsorption.

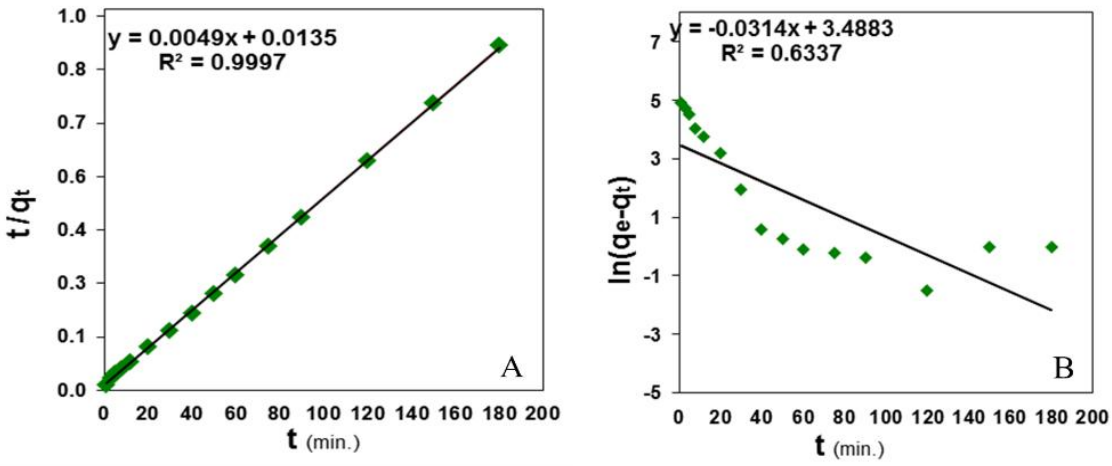

Figure 14. (A) Pseudo-second-order (B) pseudo-first-order model for R6G dye adsorption on hydrogel Surface.

Table 3. Kinetic constants for pseudo-first and pseudo-second models for R6G dye adsorption on hydrogel Surface.

Adsorbate	Pseudo-first order		
	R^2	Q_e(mg/g)	K_1 (min^{-1})
R6G	0.63	32.73	0.03
Adsorbate	**Pseudo-second order**			
	h ($mg.g^{-1}.min^{-1}$)	R^2	Q_e(mg/g)	K_2($g.mg^{-1}.min^{-1}$)
R6G	74.07	0.99	204.08	0.001

4. Conclusion

The study successfully synthesized and characterized azo-functionalized polymeric hydrogels, specifically P(AA-co-1-MeCPAI), demonstrating effective adsorption capabilities for R6G dye from aqueous solutions. Results indicate that adsorption efficiency is significantly influenced by parameters such as pH, temperature, contact time, and adsorbent dose. The adsorption process was found to be exothermic, with thermodynamic data showing a spontaneous and physical adsorption mechanism, primarily due to enthalpy values below 40 kJ/mol. Kinetic studies revealed that the adsorption follows a pseudo-second-order model, indicating the significance of chemical interactions between the dye molecules and active sites on the hydrogel surface. Additionally, isotherm analyses highlighted that the Temkin model best describes the adsorption process, suggesting that adsorption occurs in a thick monolayer structure with multilayer tendencies due to the heterogeneous nature of the hydrogel surface. This study underscores the potential of azo-functionalized hydrogels as effective adsorbents for dye removal, offering a promising approach to mitigating industrial dye pollution in water systems.

Author contributions

Authors contributed equally to the manuscript.

Acknowledgments

Authors would like to acknowledge University of Al-Qadisiyah for administrative and technical support.

Conflict of interest

The authors declare no conflict of interest

References

1. Shah A, Arjunan A, Manning G, Batool M, Zakharova J, Hawkins AJ, et al. Sequential novel use of Moringa oleifera Lam., biochar, and sand to remove turbidity, E. coli, and heavy metals from drinking water. Cleaner Water. 2024:100050.
2. Shah A, Arjunan A, Thumma A, Zakharova J, Bolarinwa T, Devi S, et al. Adsorptive removal of arsenic from drinking water using KOH-modified sewage sludge-derived biochar. Cleaner Water. 2024:100022.
3. Shah A, Zakharova J, Batool M, Coley MP, Arjunan A, Hawkins AJ, et al. Removal of cadmium and zinc from water using Sewage sludge-derived biochar. Sustainable Chemistry for the Environment. 2024.
4. Shah A, Arjunan A, Baroutaji A, Zakharova J. A review of physicochemical and biological contaminants in drinking water and their impacts on human health. Water Science and Engineering. 2023.
5. Batool M, Javed T, Wasim M, Zafar S, Din MI. Exploring the usability of Cedrus deodara sawdust for decontamination of wastewater containing crystal violet dye. Desalination and water treatment. 2021;224:433-48.
6. Bukhari A, Javed T, Haider MN. Adsorptive exclusion of crystal violet dye from wastewater by using fish scales as an adsorbent. J Dispers Sci Technol. 2022:1-12.
7. Imran MS, Javed T, Areej I, Haider MN. Sequestration of crystal violet dye from wastewater using low-cost coconut husk as a potential adsorbent. Water Sci Technol. 2022;85(8):2295-317.
8. Urooj H, Javed T, Taj MB, Nouman Haider M. Adsorption of crystal violet dye from wastewater on Phyllanthus emblica fruit (PEF) powder: kinetic and thermodynamic. International Journal of Environmental Analytical Chemistry. 2023:1-26.
9. Pavithra KG, Jaikumar V. Removal of colorants from wastewater: A review on sources and treatment strategies. Journal of Industrial and Engineering Chemistry. 2019;75:1-19.
10. Abdullah AR, Jasim LS. High-efficiency removal of diclofenac sodium (DS) drug using chitosan-grafted-poly (acrylic acid-co-N-isopropylacrylamide)/kaolin clay hydrogel composite. International Journal of Environmental Analytical Chemistry. 2024:1-21.
11. A Mahdi M, Jasim LS, O Jamel H. Removal of Rhodamine B from Aqueous Solutions Using Chitosan-g-poly (acrylic acid)/2-(((1E, 2E)-1, 2-diphenyl-2-((4 (E-1-(thiazol 2ylimino) ethyl) phenyl) imino) ethylidene) amino) phenol composite as an Adsorbent. Journal of Nanostructures. 2023.
12. Zhao S, Zhou F, Li L, Cao M, Zuo D, Liu H. Removal of anionic dyes from aqueous solutions by adsorption of chitosan-based semi-IPN hydrogel composites. Composites Part B: Engineering. 2012;43(3):1570-8.
13. Peng Q, Liu M, Zheng J, Zhou C. Adsorption of dyes in aqueous solutions by chitosan–halloysite nanotubes composite hydrogel beads. Microporous Mesoporous Mater. 2015;201:190-201.
14. Aminnezhad S, Aljelehawy QHA, Rezaei M, Mohammadi MR, Zonobian MA, Nazari M, et al. Revolutionizing medicine: Molecularly imprinted polymers as precision tools in cancer diagnosis and antibiotic detection. Cellular and Molecular Biology. 2024;70(5):100-10.
15. Abdulsahib WK, Sahib HH, Mahdi MA, Jasim LS. Adsorption Study of Cephalexin Monohydrate Drug in Solution on Poly (vinyl pyrrolidone-acryl amide) Hydrogel Surface. International Journal of Drug Delivery Technology. 2021;11(4):1169-72.
16. Radhy ND, Jasim LS. A novel economical friendly treatment approach: Composite hydrogels. Caspian Journal of Environmental Sciences. 2021;19(5):841-52.
17. Mahdi MA, Jasim LS, Mohamed MH. Synthesis and anticancer activity evaluation of novel ligand 2- [2 - (5-Chloro carboxy phenyl) Azo] 1-Methyl Imidazole (1-Mecpai) with Some Metal Complexes. Systematic Reviews in Pharmacy. 2020;11(12):1979-87.
18. Jamel HO, Jasim MH, Mahdi MA, Ganduh SH, Batool M, Jasim LS, et al. Adsorption of Rhodamine B dye from solution using 3-((1-(4-((1H-benzo[d]imidazol-2-yl)amino)phenyl)ethylidene)amino)phenol (BIAPEHB)/ P(AA-co-AM) composite. Desalination and Water Treatment. 2025:101019.
19. Majeed HJ, Idrees TJ, Mahdi MA, Abed MJ, Batool M, Yousefi SR, et al. Synthesis and application of novel sodium carboxy methyl cellulose-g-poly acrylic acid carbon dots hydrogel nanocomposite (NaCMC-g-PAAc/CDs) for adsorptive removal of malachite green dye. Desalination and Water Treatment. 2024:100822.
20. Hasan RC, Karam FF, Baqir SJ, editors. Synthesis and characterization of a novel organic reagent and its complexes with Cu (||), Cr(|||), Co(|||) and Fe(|||) metal. IOP Conference Series: Earth and Environmental Science; 2022.
21. Kmal RQ, Aljeboree AM, Jasim LS, Radia ND, Alkaim AF. Removal of Toxic Congo Red Dye from Aqueous Solution Using a Graphene Oxide/Poly (Acrylamide-Acrylic acid) Hydrogel: Characterization, Kinetics and Thermodynamics Studies. Journal of Chemical Health Risks. 2022;12(4):609-19.
22. Tang Y, Yang R, Ma D, Zhou B, Zhu L, Yang J. Removal of methyl orange from aqueous solution by adsorption onto a hydrogel composite. Polym Polym Compos. 2018;26(2):161-8.
23. Badshah I, Alam S, Shah LA, Zahoor M, Umar MN, Ullah R, et al. Adsorption and catalytic reduction of basic red 1 dye by nickel nanoparticles hydrogel: A study on kinetics, isotherm, and thermodynamics. Desalination and Water Treatment. 2024;317:100067.

24. Rehman H, Javed T, Thumma A, Uddin AN, Singh N, Baig MM, et al. Potential of easily available low-cost raw cotton for the elimination of methylene blue dye from polluted water. Desalination and Water Treatment. 2024;318:100319.
25. Rafak SH, Jasim LS. Synthesis of novel bentonite/pectin-grafted-poly (crotonic acid-co-acrylic acid) hydrogel nanocomposite for adsorptive removal of safranin O dye from aqueous solution. International Journal of Environmental Analytical Chemistry. 2024:1-24.
26. Sanad M, Farahat M, Khalek MA. One-step processing of low-cost and superb natural magnetic adsorbent: kinetics and thermodynamics investigation for dye removal from textile wastewater. Adv Powder Technol. 2021;32(5):1573-83.
27. Hayat K. Studies on Sorption of Methylene Blue over Cedrus Deodara Saw 2013.
28. Saruchi, Kumar V, Ghfar AA, Pandey S. Microwave synthesize karaya Gum-Cu, Ni nanoparticles based bionanocomposite as an adsorbent for malachite green dye: kinetics and thermodynamics. Frontiers in Materials. 2022;9:827314.